HHS Public Access

Author manuscript

Science. Author manuscript; available in PMC 2024 September 27.

Published in final edited form as:

Science. 2024 August 16; 385(6710): 738–743. doi:10.1126/science.ado5708.

A hippocampal circuit mechanism to balance memory reactivation during sleep

Lindsay A. Karaba[†],
Heath L. Robinson[†],
Ryan E. Harvey,
Weiwei Chen,
Antonio Fernandez-Ruiz,
Azahara Oliva[*]

Department of Neurobiology and Behavior, Cornell University, Ithaca, NY, USA.

Abstract

Memory consolidation involves the synchronous reactivation of hippocampal cells active during recent experience in sleep sharp-wave ripples (SWRs). How this increase in firing rates and synchrony after learning is counterbalanced to preserve network stability is not understood. We discovered a network event generated by an intrahippocampal circuit formed by a subset of CA2 pyramidal cells to cholecystokinin-expressing (CCK+) basket cells, which fire a barrage of action potentials ("BARR") during non–rapid eye movement sleep. CA1 neurons and assemblies that increased their activity during learning were reactivated during SWRs but inhibited during BARRs. The initial increase in reactivation during SWRs returned to baseline through sleep. This trend was abolished by silencing CCK+ basket cells during BARRs, resulting in higher synchrony of CA1 assemblies and impaired memory consolidation.

New memories are initially consolidated in the hippocampus during sleep after experience (1–3). As part of this process, neurons encoding a recent experience increase their firing rate during subsequent sleep sharp-wave ripples (SWRs) (4–8). Hippocampal ensembles that represent behaviorally relevant aspects of experience are reactivated together during SWRs (4–8). Disruption or enhancement of SWRs in sleep after learning results in memory impairment (9–11) or improvement (11), respectively. These elevated neuronal firing rates and ensemble reactivations rapidly return to baseline levels after experience (5, 8). However, it is not yet known how the brain achieves this rebalance after the selective potentiation of experience-related activity patterns. We hypothesized that the hippocampus

[*]**Corresponding author.**: aog35@cornell.edu.
[†]These authors contributed equally to this work.

Author contributions: Conceptualization: A.O., A.F.-R., L.A.K., H.L.R., R.E.H., and W.C.; Investigation: L.A.K., H.L.R., R.E.H., W.C., A.F.-R., and A.O.; Visualization: L.A.K. and H.L.R.; Funding acquisition: A.O. and A.F.-R.; Supervision: A.O.; Writing – original draft: A.O.; Writing – review and editing: A.O., A.F.-R., L.A.K., H.L.R., R.E.H., and W.C.

Competing interests: Authors declare that they have no competing interests.

leverages distinct circuit mechanisms to balance the increase in firing rates during memory consolidation. We thus conducted hippocampal CA1, CA2, and CA3 recordings in mice during various memory tasks and sleep (Fig. 1A and fig. S1A).

A distinct network event anticorrelated with SWRs and modulated by learning

SWRs are prominent during non–rapid eye movement (NREM) sleep, tend to occur simultaneously across hippocampal subregions (Fig. 1B), and recruit the firing of most pyramidal cells and interneurons in the hippocampus (12, 13). In addition to SWRs, we observed a different type of network event wherein a subset of CA2 pyramidal cells fired long barrages of action potentials (BARRs), coincident with an increased firing in a subset of CA1 and CA2 interneurons (Fig. 1B and figs. S1 to S3). BARRs had a longer duration than SWRs (300- versus 50-ms median duration; fig. S1J). Both SWRs and BARRs occurred mostly during NREM sleep (fig. S1D) and were anticorrelated in time (Fig. 1C and fig. S1C). Pyramidal cells in CA1, CA2, and CA3 were highly entrained during SWRs (Fig. 1D, left). A subpopulation of CA2 cells ramped (CA2ramp) their firing rate earlier and then became silenced (12, 14) (Fig. 1D, left), which was followed by the strong phasic firing of the rest of the CA2 (“CA2phas”), CA3, and CA1 cells (Fig. 1D, left). This dynamic was the opposite during BARRs; CA2ramp cells were the most active, whereas CA1 and CA3 cells did not increase their firing rates on average (Fig. 1D, right, and fig. S2, A to D). Principal components analysis of population bursts detected during SWRs, BARRs, and theta oscillations showed clearly segregated clusters (fig. S4, H and I). Overall, CA2 pyramidal cells were more bursty than CA1 (fig. S2E), with BARR-contributing CA2 cells being the most bursty of all (fig. S2F). CA2ramp cells fired long bursts of action potentials, featuring up to ~20 spikes within individual BARR events (fig. S2, H and I). Additionally, there was an anatomical segregation of CA2 pyramidal cells: Deep cells fired more in BARRs and less in SWRs, and superficial cells displayed the opposite modulation (Fig. 1E and fig. S2J). We also identified a similar modulation of interneurons. Putative parvalbumin-expressing (PV+) interneurons strongly increased their firing during SWRs but not during BARRs, whereas a different subset of interneurons was strongly recruited during BARRs but not SWRs (Fig. 1F and fig. S3).

The characteristic local field potential (LFP) oscillations at ~150 Hz during SWRs across the CA1 and CA2 pyramidal layer were absent during BARRs (Fig. 1G and fig. S2K). The firing of both pyramidal cells and interneurons was synchronized at the population level at ~150 Hz during SWRs (fig. S4, A and B) but not during BARRs (fig. S4, C and D). During BARRs, both CA2 pyramidal cells (fig. S4E) and the subset of active CA1 and CA2 interneurons (fig. S4, F and G) coordinated their firing at ~15 Hz. Despite having such distinctive spiking and LFP properties, BARR occurrence did not correlate with global brain state changes (fig. S1, K and L).

To verify whether our results extend to other species, we analyzed a dataset of hippocampal recordings in rats performing spatial memory tasks (12, 15). BARRs in rats occurred during

NREM sleep and recruited the strong firing of a subset of CA2 pyramidal cells, similar to those in mice (fig. S5).

To identify the mesoscopic signature of BARRs, we decomposed CA2 LFPs into their underlying sources using independent components analysis (ICA). ICA extracted two different sources in CA2 for SWR and BARR activity, characterized by dominant power at ~150 and ~250 Hz, respectively (fig. S6).

Next, we sought to understand whether BARRs, in addition to SWRs, were modulated by different hippocampus-dependent memory tasks. We trained mice in a delayed alternation spatial memory task (16), an object displacement memory task (17), and a social memory task (11). The incidence of both SWRs and BARRs increased during postlearning sleep for all memory tasks (Fig. 1H).

Experience-related ensemble activity is inhibited during BARRs

We aimed to understand the functional role of BARRs during memory consolidation. We focused on the CA1 region because it is the main output of the hippocampus. We first classified CA1 cells on the basis of their firing rate modulation during learning tasks and quantified their activity in SWRs and BARRs after the task, normalized by their activity in the same events during pretask sleep (“FR gain”). Neurons that selectively increased their firing rates during learning were more reactivated in posttask sleep SWRs compared with others (Fig. 2A, left). These “task-active” cells decreased their firing rates during posttask BARRs more than other cells (Fig. 2A, right). Similarly, CA1 place cells (fig. S7, A to C) increased their firing rates more during postsleep SWRs compared with nonplace cells (Fig. 2B, left) and decreased their firing rate during postsleep BARRs more than nonplace cells (Fig. 2B, right). Both CA2 BARR+ and CA2 BARR− pyramidal cells displayed spatial modulation (fig. S7, D and E) and formed assemblies during behavior that were differentially modulated by SWRs and BARRs (fig. S7, F and G).

The firing rate gain of individual CA1 neurons in SWRs and BARRs was anticorrelated (Fig. 2C). Cells that increased their firing rates more in SWRs from pre- to postlearning sleep were the most silenced during BARRs (Fig. 2C and fig. S8A). However, thesameanalysis applied to REM epochs (fig. S8B) or random periods of NREM sleep (fig. S8C) showed a positive correlation. This firing rate modulation also had a Characteristic temporal dynamic. Firing rates of task-active cells were more elevated in early SWRs and gradually decreased (Fig. 2D) with the amount of NREM sleep (fig. S8H). On the contrary, cells were more strongly suppressed in BARRs at the beginning of sleep and increased their firing rate over a similar timescale (Fig. 2D). Next, we detected CA1 assemblies during learning (11, 18–20) and found that these assembly patterns were significantly reactivated during postsleep SWRs (Fig. 2E, left, and fig. S8, D to F). By contrast, the same assembly patterns were significantly suppressed during postsleep BARRs (Fig. 2E, right, and fig. S8, D to F). We also calculated the explained variance (EV) (5, 11, 19, 20) and found a robust increase in CA1 pyramidal cells’ EV during SWRs but a decrease during BARRs (Fig. 2F).

To mimic a learning-induced increase in SWR incidence, we artificially generated SWRs (11, 21, 22). We delivered 100-ms blue light pulses to the CA1 region of CamKII::ChR2 mice (Fig. 2, G and H) (11, 21) at 0.2 Hz for 2 hours while mice rested in their home cage, which resulted in an increase in SWR incidence during this period (fig. S8G). The stimulation session was preceded and followed by rest periods of 2 hours (Fig. 2G). BARR rate increased in the poststimulation period compared with baseline, whereas SWRs maintained a similar rate (Fig. 2I). Furthermore, CA1 pyramidal cells that increased their firing rate during artificially generated SWRs decreased their firing rate during poststimulation BARRs (Fig. 2J).

Similarly in rats, posttask firing rate gain in SWRs and BARRs was anticorrelated, and place cells were more inhibited in BARRs than nonplace cells (fig. S8, I and J).

Distinct interneuron subtypes modulate SWRs and BARRs

To elucidate the mechanism that supports the selective inhibition of CA1 firing during BARRs, we compared the electrophysiological properties of the different interneuron subpopulations that were most active during SWRs (putative PV+ cells) (21, 23, 24) and BARRs (BARR+ interneurons) (Fig. 1F). Putative PV+ interneurons had narrow waveforms and short refractory periods (Fig. 3A) and were highly active during SWRs (21, 23, 24) but not during BARRs (Fig. 1F). By contrast, BARR+ interneurons had wider waveforms and longer refractory periods (Fig. 3A) and were suppressed or only weakly active during SWRs (Fig. 1F). Both cell types showed different state-dependent firing. Putative PV+ interneurons fired more during periods of running than immobility and more during theta oscillations compared with nontheta waking periods, whereas BARR+ interneurons displayed the opposite modulation (Fig. 3B and fig. S3J). These properties were consistent with features of a subset of hippocampal basket cells that express cholecystokinin (CCK+) (25, 26), targeted by the selective expression of the SNCG promoter (Sncg+ cells). Therefore, we hypothesized that BARR+ interneurons largely overlap with this genetically defined interneuron subtype. We injected Flp-dependent channelrhodopsin (ChR2) in the CA1 region of Sncg-Flp mice (25) to specifically express ChR2 in Sncg+ cells (fig. S3K). Applying long-duration (~500 ms) blue light pulses resulted in a decreased firing rate of CA1 pyramidal cells (fig. S9A). Next, we identified Sncg+ cells (putative CCK+ basket cells) from their spiking response to blue or green light pulses [in Sncg-Flp mice expressing Flp-dependent ChR2 or archaerhodopsin (Arch), respectively] (fig. S3, K and L). Optogenetically identified Sncg+ cells were highly active during BARRs but not during SWRs, and they preferred firing during awake immobility periods compared with awake theta periods (Fig. 3, C and D). The waveforms and autocorrelograms of identified Sncg+ cells were similar to those of the previously identified BARR+ interneurons (fig. S9, B to E). In addition, a *t*-distributed stochastic neighbor embedding (t-SNE) analysis of physiological properties comparing all interneuron groups revealed a large overlap of Sncg+ cells and BARR+ interneurons subgroups (Fig. 3E), which supports our hypothesis that many BARR+ interneurons were CCK+ basket cells. Of note, although the main group of BARR+ interneurons overlapped with optogenetically identified Sncg+, other BARR+ cells were scattered outside this main group. On the basis of their low or negative modulation by

SWRs and locomotion speed, these cells could correspond to axo-axonic (26) or vasoactive intestinal peptide–expressing (VIP+) (27) interneurons.

CA2 and CCK+ basket cells form an anatomically defined functional circuit

Next, we assessed whether CA2 pyramidal cells and CA1 Sncg+ interneurons form a functionally connected anatomical circuit, given their entrainment during BARRs. We used a set of viral-genetic strategies based on rabies-virus tracing of presynaptic partners of specific cellular subtypes (28–30) (Fig. 4A). We validated the infection of Sncg+ cells (Fig. 4B, red arrows) and identified starter cells (Fig. 4, B and C, yellow arrows) as well as their direct inputs (eGFP+/Sncg−; Fig. 4, B and C, green arrows), which clustered in the CA2 region of the hippocampus. Quantification of input cells to CA1 Sncg+ interneurons across animals revealed that a higher proportion of the inputs were from CA2 pyramidal cells (Fig. 4D and fig. S10). To validate this anatomical circuit in vivo, we identified putative monosynaptic connections by short-lag (2 to 3 ms) peaks in pyramidal cell–interneuron spike train cross-correlograms (31) (Fig. 4, E and F). CA2 pyramidal cells had a higher proportion of monosynaptic connections with CA1 BARR+ than with PV+ interneurons (Fig. 4E), whereas CA1 pyramidal cells had a higher proportion of connections with CA1 PV+ interneurons than with BARR+ interneurons (Fig. 4F). In addition, silencing CA2 pyramidal cells in Amigo2-Cre animals injected with Cre-dependent Arch3.0 also decreased firing rate in putative Sncg+ interneurons in CA1 (fig. S10, F and G).

Silencing Sncg+ cells during consolidation impairs memory

We assessed whether BARRs, in addition to SWRs (4–12), are also necessary for memory consolidation. We disrupted the specific BARR-associated inhibition of CA1 by silencing Sncg+ cells (fig. S10E). To optimize the silencing to specific BARR periods, we calculated the timing from each BARR to the nearest preceding SWR, which displayed an average peak distance of ~2 s (Fig. 5, A and B). We recorded Sncg-Flp mice injected with Flp-dependent Arch in the CA1 region during an object displacement memory task (fig. S1A). During postsleep periods, we detected SWRs and, 2 s after, delivered 2-s green light pulses to silence Sncg+ firing (fig. S10E) and disrupt BARR-associated inhibition of CA1 pyramidal cells (“BARR disruption”). SWR properties did not change during light activation of Sncg+ cells (fig. S9, G to J), nor did the overall SWR rate increase from pre- to postsleep (Fig. 5C). Furthermore, the reactivation of task-related assemblies in SWRs was also preserved (Fig. 5D). Yet this manipulation impaired memory performance (Fig. 5E). By contrast, closed-loop silencing of Sncg+ cells during SWRs did not affect memory performance (Fig. 5E). Additionally, in control sessions, the firing rate gain during SWRs increased in the first ~30 min of postlearning sleep and rapidly went back to baseline. On the contrary, in BARR disruption sessions, the firing rate gain during SWRs remained elevated during postlearning sleep (Fig. 5F). Population synchrony was also elevated in BARR disruption compared with control sessions (Fig. 5, G and H).

Discussion

The present results expand our understanding of the hippocampal mechanisms of memory consolidation by identifying a network event (BARR) wherein specific neurons that encoded a recent experience became inhibited. BARR events consisted of periods of persistent firing of a subset of deep-sublayer CA2 pyramidal cells along with an increased firing of Sncg+ cells (putative CCK+ basket cells). They occurred during NREM sleep and increased in rate after learning.

BARRs selectively inhibited task-related CA1 pyramidal cells in an activity-dependent manner. The more reactivated a given cell was during the learning and, subsequently, during postsleep SWRs, the more it was inhibited during BARRs. Similarly, assembly coactivity patterns that formed during learning were reactivated in subsequent sleep SWRs but inhibited during BARRs. Optogenetic disruption of BARRs after learning impaired memory performance. Although this manipulation did not affect the incidence of SWRs, it resulted in higher firing rates and synchrony for CA1 assemblies during SWRs, in line with recent results (32). This suggests that an optimal and dynamic range of assembly reactivation is required for memory consolidation, with a lack of reactivation (such as during SWRs disruption) or hypersynchronous reactivation (such as during pathological conditions) resulting in memory deficits. Furthermore, our findings show that BARRs play a homeostatic role in balancing SWR-associated neuronal reactivation. Our results were replicated for several types of memory tasks and different species, indicating that BARRs are a general hippocampal mechanism that contributes to memory consolidation. This mechanism could prevent firing rates and synchrony from continuously increasing over time because of the enhanced cell recruitment during SWRs and overall postsleep firing rate increase (4–12), which could otherwise reach a pathological regime (33, 34).

Various physiological mechanisms have been identified in support of the homeostatic role of sleep (35) at the cellular (36), synaptic (37), and neuronal population levels (38–40). However, it is not yet understood how the selective reactivation of coactive task-relevant assemblies during sleep SWRs is related to the synaptic homeostasis theory of sleep (35). It has been suggested that the reactivation of specific cell assemblies can only occur alongside a decrease in the firing rate of other assemblies, so the overall network firing rates are balanced (41). An alternative hypothesis is that complementary mechanisms (SWRs and BARRs) reactivate and inhibit the same task-related assemblies. Our data support the latter, as the same assemblies are up- and down-modulated during SWRs and BARRs, respectively. In favor of this idea, it was recently shown that SWRs are necessary for the hippocampus to express long-term depression during sleep (42). Our results provide experimental evidence that can help reconcile memory consolidation models (41) and the synaptic homeostasis hypothesis of sleep (35).

We previously showed that CA2 deep-sublayer pyramidal cells became rapidly silenced during SWRs (11, 12). In addition, a subset of CA2 pyramidal cells has been shown to become highly active during immobility and later on during sleep, likely corresponding to the same CA2 ramping population (12, 14) and probably to BARR+ CA2 cells. A similar response was observed in CA1 CCK+ basket cells (25, 26). CA1 pyramidal cells from deep

and superficial sublayers send distinct information to different cortical areas (19), emerge at different developmental stages (43, 44), and have different physiological and functional correlates (19, 43–47). Our results suggest that a deep-superficial functional organization also exists in CA2, with superficial CA2 cells being highly active during SWRs and deep CA2 firing more during BARRs. Therefore, CA2 could act as a hub to set the network state (SWRs or BARRs) within the hippocampus. The selectivity of which cells are to be recruited during SWRs and BARRs could be supported by genetically distinct interneuron subtypes locally in CA1. PV+ interneurons contribute to the timing and coordination of cell assemblies during SWRs (21, 48). However, we showed that CCK+ basket cells were highly active during BARRs but not during SWRs. CCK+ basket cells express receptors for cannabinoids (CB1) (49, 50), retrograde messengers that can be activated by burst-like firing of CA1 pyramidal cells (51). Cannabinoid release after CA1 pyramidal cell firing during SWRs, possibly also aided by PV disinhibition (25, 50), could recruit CCK+ firing, which would then inhibit cells that are more active after learning.

Experimental and theoretical work has suggested that, in neocortical structures, network homeostasis is maintained by the balanced firing rates of the overall population (38, 40). In the hippocampus, we showed that generating artificial SWRs resulted in more BARRs. Population activity recruited during SWRs propagates through the network via lateral inhibition (52) or through entorhinal cortex (15), which could provide accumulated feedforward excitation into CA2, resulting in the generation of more BARRs.

Supplementary Material

Refer to Web version on PubMed Central for supplementary material.

ACKNOWLEDGMENTS

We thank members of the Oliva and Fernandez-Ruiz laboratories and F. Leroy for useful comments on the manuscript and M. R. Warden for providing access to the confocal microscope.

Funding:

National Institutes of Health (grants R00MH122582 and R01MH130367 to A.O. and grants 4R00MH120343 and DP2MH136496 to A.F.-R.); New Frontiers grant (to A.O.); Sloan Fellowship (to A.F.-R.); Whitehall Research Grant (to A.F.-R.); Klingenstein-Simons Fellowship (to A.F.-R.); National Science Foundation Graduate Research Fellowship (grant DGE-2139899 to L.A.K.); National Institutes of Health, Ruth L. Kirschstein National Research Service Award Individual Postdoctoral Fellowship (F32MH134673 to H.L.R.).

Data and materials availability:

All data are available in the main text or the supplementary materials. Custom scripts used in this study can be downloaded from https://github.com/ayalab1/neurocode and Zenodo (53).

REFERENCES AND NOTES

1. Scoville WB, Milner B, J. Neurol. Neurosurg. Psychiatry 20, 11–21 (1957). [PubMed: 13406589]
2. Andersen P, Morris R, Amaral D, Bliss T, O'Keefe J, Eds., The Hippocampus Book (Oxford Univ. Press, 2007).
3. Diekelmann S, Born J, Nat. Rev. Neurosci. 11, 114–126 (2010). [PubMed: 20046194]
4. Wilson MA, McNaughton BL, Science 265, 676–679 (1994). [PubMed: 8036517]

5. Kudrimoti HS, Barnes CA, McNaughton BL, Neurosci J. 19, 4090–4101 (1999).
6. Lee AK, Wilson MA, Neuron 36, 1183–1194 (2002). [PubMed: 12495631]
7. Grosmark AD, Buzsáki G, Science 351, 1440–1443 (2016). [PubMed: 27013730]
8. Giri B, Miyawaki H, Mizuseki K, Cheng S, Diba K, Neurosci J. 39, 866–875 (2019).
9. Girardeau G, Benchenane K, Wiener SI, Buzsáki G, Zugaro MB, Nat. Neurosci. 12, 1222–1223 (2009). [PubMed: 19749750]
10. Ego-Stengel V, Wilson MA, Hippocampus 20, 1–10 (2010). [PubMed: 19816984]
11. Oliva A, Fernández-Ruiz A, Leroy F, Siegelbaum SA, Nature 587, 264–269 (2020). [PubMed: 32968277]
12. Oliva A, Fernández-Ruiz A, Buzsáki G, Berényi A, Neuron 91, 1342–1355 (2016). [PubMed: 27593179]
13. Csicsvari J, Hirase H, Czurkó A, Mamiya A, Buzsáki G, Neurosci J. 19, 274–287 (1999).
14. Kay K et al., Nature 531, 185–190 (2016). [PubMed: 26934224]
15. Fernández-Ruiz A et al., Science 372, eabf3119 (2021). [PubMed: 33795429]
16. Valero M et al., Nat. Neurosci. 24, 401–411 (2021). [PubMed: 33619404]
17. Genzel L et al., PLOS Biol. 17, e3000322 (2019). [PubMed: 31206519]
18. Dupret D, O'Neill J, Pleydell-Bouverie B, Csicsvari J, Nat. Neurosci. 13, 995–1002 (2010). [PubMed: 20639874]
19. Harvey RE, Robinson HL, Liu C, Oliva A, Fernandez-Ruiz A, Neuron 111, 2076–2090.e9 (2023). [PubMed: 37196658]
20. Liu C, Todorova R, Tang W, Oliva A, Fernandez-Ruiz A, Science 382, eadi8237 (2023). [PubMed: 37856604]
21. Stark E et al., Neuron 83, 467–480 (2014). [PubMed: 25033186]
22. Fernández-Ruiz A et al., Science 364, 1082–1086 (2019). [PubMed: 31197012]
23. Gan J, Weng SM, Pernía-Andrade AJ, Csicsvari J, Jonas P, Neuron 93, 308–314 (2017). [PubMed: 28041883]
24. English DF et al., J. Neurosci. 34, 16509–16517 (2014). [PubMed: 25471587]
25. Dudok B et al., Neuron 109, 997–1012.e9 (2021). [PubMed: 33529646]
26. Vancura B, Geiller T, Grosmark A, Zhao V, Losonczy A, Nat. Neurosci. 26, 788–797 (2023). [PubMed: 37081295]
27. Turi GF et al., Neuron 101, 1150–1165.e8 (2019). [PubMed: 30713030]
28. Schwarz LA et al., Nature 524, 88–92 (2015). [PubMed: 26131933]
29. Miyamichi K et al., Neuron 80, 1232–1245 (2013). [PubMed: 24239125]
30. Wickersham IR et al., Neuron 53, 639–647 (2007). [PubMed: 17329205]
31. English DF et al., Neuron 96, 505–520.e7 (2017). [PubMed: 29024669]
32. Rangel Guerrero DK et al., Neuron 112, 2045–2061.e10 (2024). [PubMed: 38636524]
33. Valero M et al., Neuron 94, 1234–1247.e7 (2017). [PubMed: 28641116]
34. Gelinas JN, Khodagholy D, Thesen T, Devinsky O, Buzsáki G, Nat. Med. 22, 641–648 (2016). [PubMed: 27111281]
35. Tononi G, Cirelli C, Brain Res. Bull. 62, 143–150 (2003). [PubMed: 14638388]
36. Turrigiano GG, Leslie KR, Desai NS, Rutherford LC, Nelson SB, Nature 391, 892–896 (1998). [PubMed: 9495341]
37. Vyazovskiy VV, Cirelli C, Pfister-Genskow M, Faraguna U, Tononi G, Nat. Neurosci. 11, 200–208 (2008). [PubMed: 18204445]
38. Hengen KB, Torrado Pacheco A, McGregor JN, Van Hooser SD, Turrigiano GG, Cell 165, 180–191 (2016). [PubMed: 26997481]
39. Levenstein D et al., bioRxiv 2021.09.20.461152 [Preprint] (2022); 10.1101/2021.09.20.461152.
40. Watson BO, Levenstein D, Greene JP, Gelinas JN, Buzsáki G, Neuron 90, 839–852 (2016). [PubMed: 27133462]
41. Buzsáki G, Hippocampus 25, 1073–1188 (2015). [PubMed: 26135716]
42. Norimoto H et al., Science 359, 1524–1527 (2018). [PubMed: 29439023]

43. Cavalieri D et al., eLife 10, e69270 (2021). [PubMed: 34723790]
44. Huszár R, Zhang Y, Blockus H, Buzsáki G, Nat. Neurosci. 25, 1201–1212 (2022). [PubMed: 35995878]
45. Mizuseki K, Diba K, Pastalkova E, Buzsáki G, Nat. Neurosci. 14, 1174–1181 (2011). [PubMed: 21822270]
46. Valero M et al., Nat. Neurosci. 18, 1281–1290 (2015). [PubMed: 26214372]
47. Danielson NB et al., Neuron 91, 652–665 (2016). [PubMed: 27397517]
48. Schlingloff D, Káli S, Freund TF, Hájos N, Gulyás AI, Neurosci J. 34, 11385–11398 (2014).
49. Bartos M, Elgueta C, Physiol J. 590, 669–681 (2012).
50. Dudok B et al., Science 383, 967–970 (2024). [PubMed: 38422134]
51. Chevaleyre V, Castillo PE, Neuron 38, 461–472 (2003). [PubMed: 12741992]
52. McKenzie S et al., Neuron 109, 1040–1054.e7 (2021). [PubMed: 33539763]
53. Harvey R et al., Zenodo (2023); 10.5281/zenodo.7819979.

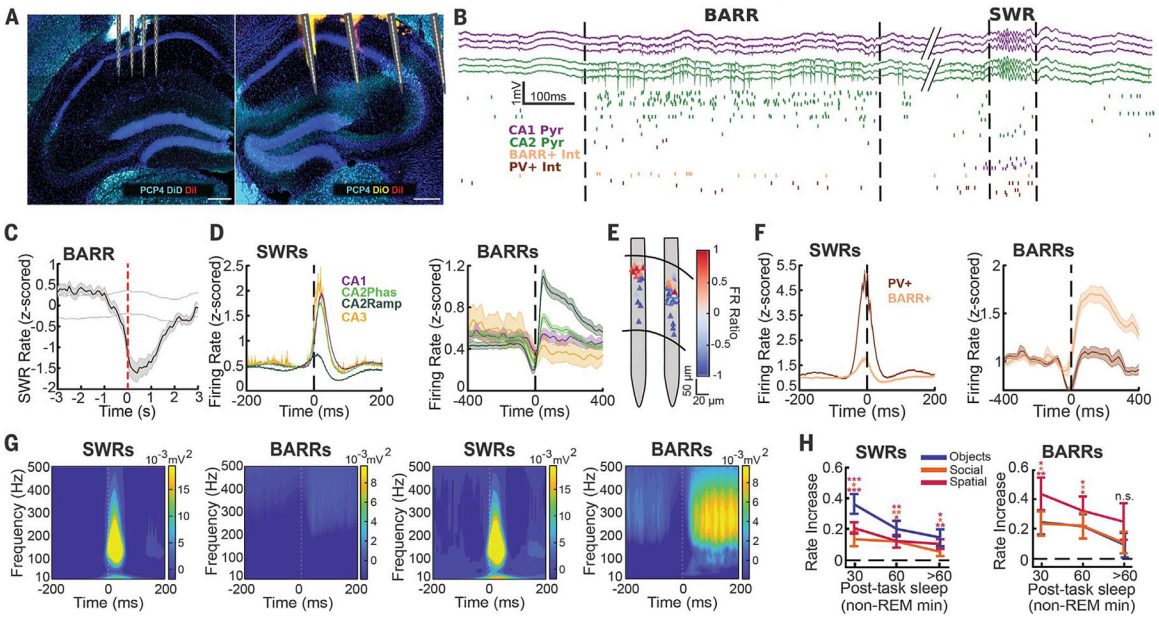

Fig. 1. A hippocampal network pattern with distinctive cellular contribution.

(**A**) Histology of bilateral electrophysiological recordings of all hippocampal subregions. DiD, 1,1′-dioctadecyl-3,3,3′3′-tetramethylindodicarbocyanine, 4-chlorobenzenesulfonate salt; DiI, 1,1′-dioctadecyl-3,3,3′,3′-tetramethylindocarbocyanine perchlorate; DiO, 3,3-′dioctadecyloxacarbocyanine perchlorate; PCP4, Purkinje cell protein 4. DiD, DiI, and DiO were used for electrode localization; PCP4 was used as a CA2 marker. (**B**) Recording of a BARR and a SWR (delimited by dashed lines). (Top) CA1 and CA2 pyramidal layer wide-band LFP traces. (Bottom) Raster plot of firing from different neuronal subtypes (each row shows a different neuron, and each tick mark is one spike). Int, interneuron; Pyr, pyramidal cell. (**C**) Averaged cross-correlogram between BARRs and SWRs (n = 52 sessions from n = 10 mice). Dashed lines indicate 95% confidence interval (CI) from shuffled data (P < 0.001, Wilcoxon rank sum test). (**D**) Averaged peri-event firing rate curves for CA1 (n = 998), CA2phas (n = 1650), CA2ramp (n = 339), and CA3 (n = 105) pyramidal cells during SWRs (left) and BARRs (right), from n = 10 mice. (**E**) Firing rate ratio [(BARR FR − SWR FR)/(BARR FR + SWR FR)] between BARRs and SWRs for cells from one session (red indicates higher firing during BARRs; blue indicates higher firing during SWRs) noted at their soma location. FR, firing rate. (**F**) Same as in (D) for putative PV+ (n = 157) and BARR active (n = 72) interneurons. (**G**) Wavelet spectrogram of SWRs (left) and BARRs (right) for CA1 (left two panels) and CA2 (right two panels) for one session. (**H**) Increase in the rate of SWRs (left) and BARRs (right) in postlearning sleep compared with prelearning sleep for the three different memory tasks (n = 23 sessions from n = 8 mice for object displacement, n = 16 sessions from n = 7 mice for social memory, n = 14 sessions from n = 4 mice for T-Maze. *P < 0.05; **P < 0.01; ***P < 0.001; n.s., not significant; signed-rank test). Data are shown as mean ± SEM.

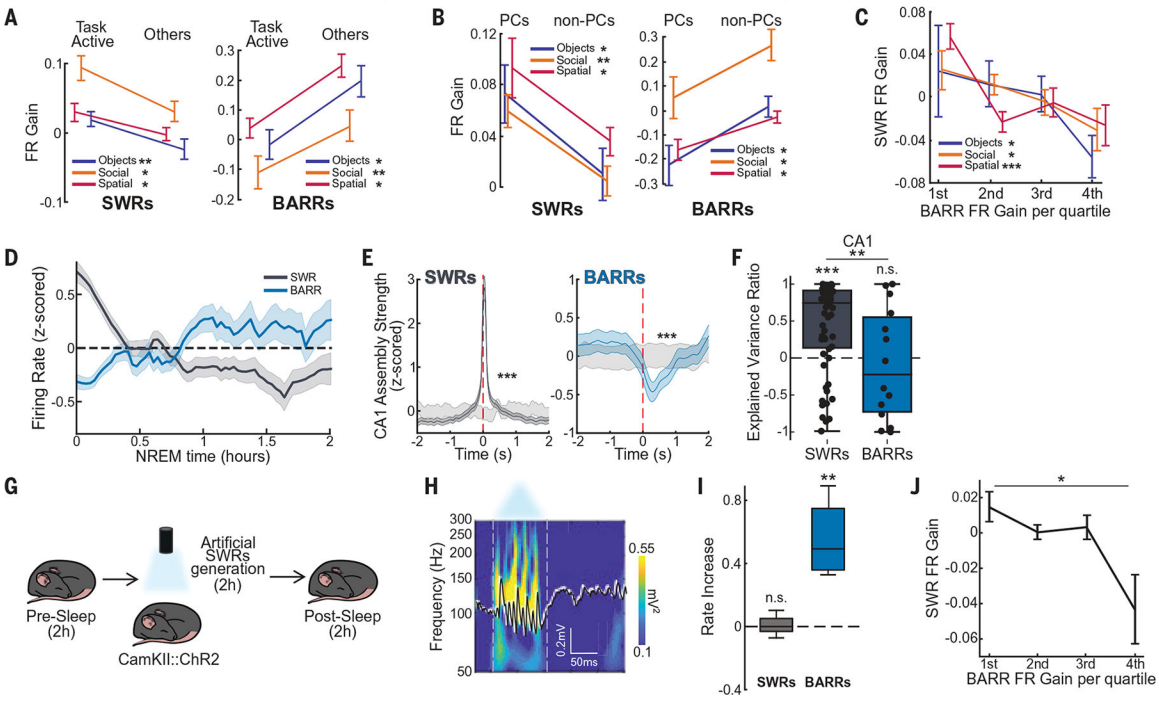

Fig. 2. BARRs inhibit task-active cells and assemblies.

(**A**) Firing rate gain of cells most active during learning ("task active") versus the rest of pyramidal cells ("others"), during SWRs and BARRs (n = 124/241, n = 102/130, and n = 140/237 task-active/other cells for Objects, Social, and T-Maze task, respectively). (**B**) Firing rate gain during SWRs and BARRs for CA1 PCs (n = 34/141, n = 36/128, and n = 313/447 PCs/non-PCs for Objects, Social, and T-Maze task, respectively). PC, place cell. (**C**) CA1 pyramidal cell firing rate gain during SWRs sorted by their firing rate gain in BARRs (quartiles) for each task (n = 185, 164, and 327 cells for Objects, Social, and T-Maze task, respectively; *P < 0.05; **P < 0.01; ***P < 0.001; linear regression). (**D**) Firing rate evolution over time in SWRs (gray) and BARRs (blue) for cells that showed a higher increase in SWRs after the task [P < 0.001, analysis of variance (ANOVA) of type of event, SWRs and BARRs, versus time interaction]. For (A) to (D), n = 22 sessions, n = 8 mice for Objects task; n = 15 sessions, n = 7 mice for Social task; n = 16 sessions, n = 4 mice for T-Maze task. (**E**) Averaged CA1 assembly reactivation during postlearning sleep SWRs (left) and BARRs (right) compared with shuffled periods (light gray) (n = 72, 41, and 42 assemblies for Objects, Social, and T-Maze task, respectively). (**F**) CA1 explained variance ratio [(EV−REV)/(EV+REV)] in postlearning sleep SWRs (n = 59 sessions) and BARRs (n = 14 sessions). EV, explained variance. REV, reversed explained variance. (**G**) Schematic of optogenetic SWR generation. (**H**) Example of artificially generated CA1 SWR. (**I**) SWR and BARR rate during the poststimulation period compared with the preceding baseline period (P > 0.05 and P < 0.01 for SWR and BARR rate increase, respectively; n = 4 mice, n = 9 sessions). (**J**) CA1 pyramidal cells firing rate gain during BARRs versus SWRs from pre– to postartificial SWRs (quartiles) (n = 148 cells, P < 0.05, linear regression). *P < 0.05; **P < 0.01; ***P < 0.001; Wilcoxon rank sum test unless otherwise noted.

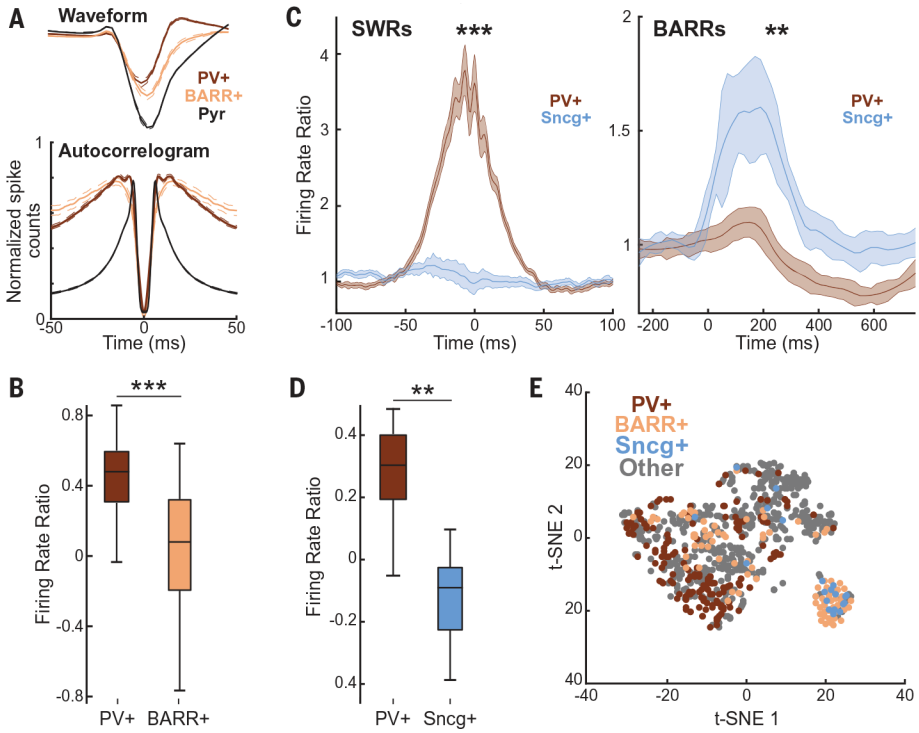

Fig. 3. Sncg+ cells are entrained by BARRs.

(**A**) (Top) Average waveforms of PV+, BARR+ interneurons, and pyramidal cells (for comparison) (n = 157, 72, and 998 for PV+, BARR+, and pyramidal cells, respectively; n = 10 mice; P < 0.001 for PV+ versus BARR+ waveform width comparison). (Bottom) Averaged normalized autocorrelograms of PV+, BARR+ interneurons, and pyramidal cells (P < 0.001 for PV+ versus BARR+ burstiness comparison). (**B**) Firing rate difference during periods of running and immobility for PV+ and BARR+ interneurons (P < 0.001). (**C**) Firing modulation of Sncg+ cells and putative PV+ cells (n = 20/33, respectively, from n = 10 sessions in n = 3 mice) during SWRs (left) and BARRs (right). (**D**) Firing rate difference during periods of running and immobility for PV+ and Sncg+ interneurons. (**E**) t-SNE of waveform and firing properties of different interneuron subtypes (from n = 13 mice: PV+, n = 172; BARR+, n = 94; Sncg+, n = 20; other interneurons, n = 510). *P < 0.05; **P < 0.01; ***P < 0.001; Wilcoxon rank sum test unless otherwise noted.

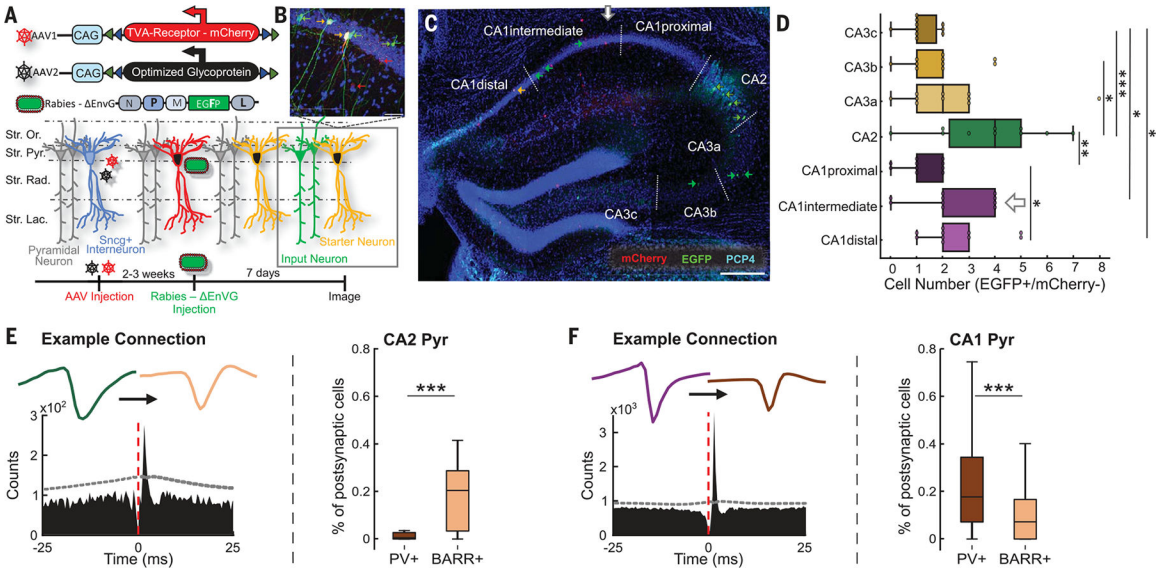

Fig. 4. CA2 to Sncg+ cells form an anatomically defined circuit.

(**A**) Schematic of viral strategy used to label monosynaptically projecting cells onto Sncg+ cells. First, an AAV-TVA (AAV, adeno-associated virus; TVA, tumor virus A) cocktail targeting specific cell types (Sncg+) was injected. Next, a G protein–deleted rabies-dependent virus was injected to retrogradely label the presynaptic partners of Sncg+ cells. EGFP, enhanced green fluorescent protein; Str. Lac., stratum lacunosum moleculare; Str. Or., stratum oriens; Str. Pyr., stratum pyramidale; Str. Rad., stratum radiatum. (**B**) Example of cells labeled as starter neurons (yellow cells), with additional labeling of input neurons (green cells) and Sncg+ interneurons (red cells). Blue: 4′,6-diamidino-2-phenylindole staining. (**C**) Histology showing AAV-infected cells (red), starter cells (yellow), and input cells (green). Dashed lines delimit hippocampal regions. CA2 is labeled in cyan with PCP4. Horizontal bar = 300 μm. (**D**) Quantification of cells identified as input cells (EGFP+/mCherry−) from different subregions of the hippocampus (*$P < 0.05$; **$P < 0.01$; ***$P < 0.001$; ANOVA with Dunn's post hoc test, $n = 11$ slices from $n = 4$ mice). (**E**) (Left) Cross-correlograms of putatively monosynaptically connected CA2 pyramidal cell (green) and BARR+ interneuron (peach color), with their respective waveforms. Dashed line indicates CIs ($\alpha = 0.001$). (Right) Relative proportion of CA2 pyramidal cell functional monosynaptic inputs into CA1 BARR+ and PV+ interneurons ($P < 0.001$; $n = 170$ CA2-BARR+ pairs and 70 CA2-PV+ pairs). (**F**) (Left) CA1 pyramidal cell (purple) and PV+ interneuron (brown) cross-correlogram and waveforms. (Right) Relative proportion of CA1 pyramidal cell inputs into CA1 BARR+ and PV+ interneurons ($P < 0.001$; $n = 276$ CA1-BARR+ pairs and 666 CA1-PV+ pairs). *$P < 0.05$; **$P < 0.01$; ***$P < 0.001$; Wilcoxon rank sum test unless otherwise noted.

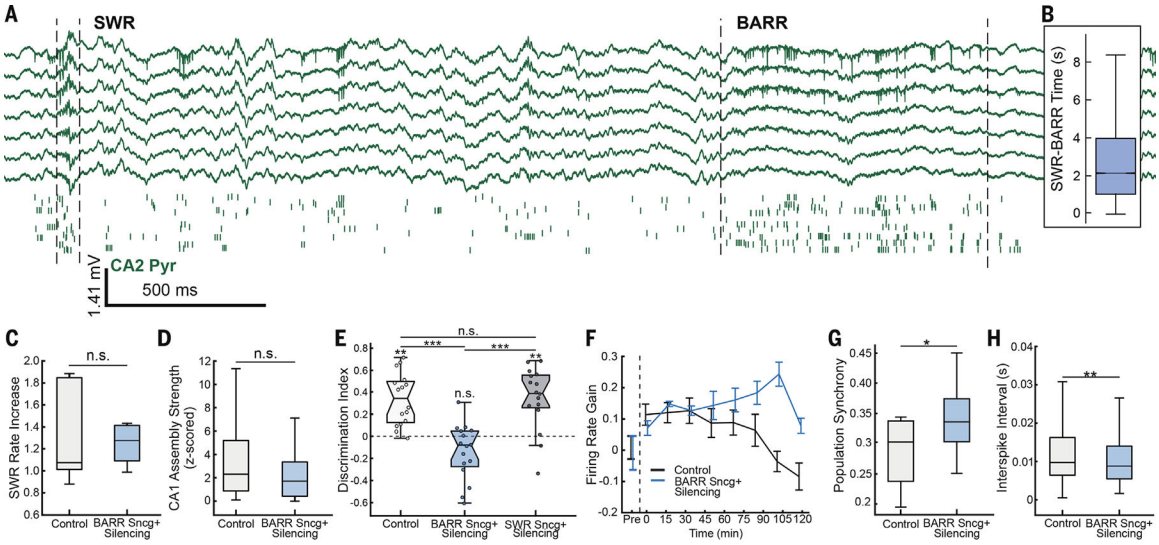

Fig. 5. BARRs are necessary for memory consolidation.

(**A**) Example recording showing ~2-s delay between an SWR and BARR. (Top) CA2 wide-band LFP traces. (Bottom) Raster plot of firing from CA2 pyramidal cells (each row shows a different neuron, and each tick mark is one spike). (**B**) Quantification of average distance from BARRs to the previous preceding SWR, restricted to a maximum of 10-s lag time (n = 45,301 BARRs and n = 464,828 SWRs from 52 sessions in n = 10 mice). (**C**) SWR rate increase from pre- to postlearning sleep for control and Sncg+ silencing groups (n = 16 sessions in n = 8 mice; $P > 0.05$; Wilcoxon rank sum test). (**D**) Mean CA1 assembly reactivation strength during SWRs for control and Sncg+ silencing groups (n = 50 and 52 assemblies in control and Sncg+ groups, respectively; $P > 0.05$; Wilcoxon rank sum test). (**E**) Memory recall performance (discrimination index) for mice in the object displacement task without manipulation (control, light gray), Sncg+ silencing during BARR periods (BARR Sncg+ silencing, blue), and Sncg+ silencing during SWRs (SWR Sncg+ silencing, dark gray) (**$P < 0.01$; ***$P < 0.001$; ANOVA with Dunn's post hoc test for between-group comparison and Wilcoxon signed-rank for within-group comparison; n = 16 sessions per group in n = 8 mice). (**F**) Firing rate gain of CA1 pyramidal cells during SWRs in postlearning sleep for control and Sncg+ silencing sessions ($P < 0.001$ for between-group comparison and $P < 0.05$ for time effect; repeated-measures ANOVA; n = 273 and 210 cells in control and Sncg+ groups, respectively; n = 13 sessions in n = 8 mice for control and n = 11 sessions in n = 8 mice for Sncg+ group). (**G**) CA1 population synchrony in SWRs ($P <$ 0.01; t test; n = 13 sessions in n = 8 mice for control and n = 11 sessions in n = 8 mice for Sncg+ group). (**H**) Interspike interval within SWRs for control and Sncg+ silencing groups ($P < 0.01$; Wilcoxon rank sum test; n = 509 and 426 events in control and Sncg+ groups, respectively; n = 13 sessions in n = 8 mice for control and n = 11 sessions in n = 8 mice for Sncg+ group). *$P < 0.05$; **$P < 0.01$; ***$P < 0.001$; Wilcoxon rank sum test unless otherwise noted.